Implosion of multilayered cylindrical targets driven by intense heavy ion beams

A. R. Piriz and R. F. Portugues
ETSI Industriales, Universidad de Castilla-La Mancha, 13071 Ciudad Real, Spain

N. A. Tahir
Institut für Theoretische Physik, Universität Frankfurt, 60054 Frankfurt, Germany

D. H. H. Hoffmann
Institut für Kernphysik, Technische Universität Darmstadt, 64289 Darmstadt, Germany, and GSI Darmstadt, Planckstrasse 1, 64291 Darmstadt, Germany

(Received 27 June 2002; published 11 November 2002)

An analytical model for the implosion of a multilayered cylindrical target driven by an intense heavy ion beam has been developed. The target is composed of a cylinder of frozen hydrogen or deuterium, which is enclosed in a thick shell of solid lead. This target has been designed for future high-energy-density matter experiments to be carried out at the Gesellschaft für Schwerionenforschung, Darmstadt. The model describes the implosion dynamics including the motion of the incident shock and the first reflected shock and allows for calculation of the physical conditions of the hydrogen at stagnation. The model predicts that the conditions of the compressed hydrogen are not sensitive to significant variations in target and beam parameters. These predictions are confirmed by one-dimensional numerical simulations and thus allow for a robust target design.

DOI: 10.1103/PhysRevE.66.056403 PACS number(s): 51.50.+v, 25.75.−q, 62.50.+p, 79.20.Rf

I. INTRODUCTION

Study of hydrogen under extreme conditions (supersolid densities and multimegabar pressures) is of great interest to astrophysics, planetary sciences, and inertial fusion. Another very interesting aspect of this problem is the possibility of creating metallized hydrogen in laboratory by application of extremely high pressures to small samples of hydrogen [1–6]. Production of metallized hydrogen in reproducible experiments will not only provide insight to the structure of the giant planets, but may also have significant impact on our daily lives as it is expected that the metallic state of hydrogen has a number of potential industrial applications [7].

During the past decades the high-pressure technology has been significantly advanced by the development of diamond anvil cell, high power pulsed lasers, and gas guns. Moreover, high power explosives and nuclear explosive devices have also been employed to generate ultrahigh pressures. In addition to that, beams of light ions have also been recognized as a powerful tool for the production of solid density, high-pressure plasmas [8].

An additional tool that has also been available for some time to research this field is an intense heavy ion beam at the Gesellschaft für Schwerionenforschung (GSI), Darmstadt. The GSI has a heavy ion synchrotron, SIS18 which delivers intense heavy ion beams of different ion species. Important experimental work has been done in the field of high-energy-density (HED) matter using these beams during the past decade [9–13]. This facility at present is being upgraded and it is expected that after the completion of this upgrade the beam intensity will increase significantly while the pulse length will be substantially reduced (to about 50 ns). Detailed numerical simulations have shown [14–16] that using this future beam, one will be able to access much wider regions of the parameter space of the physical conditions of the HED matter. These simulations have been done using a two-dimensional hydrodynamic model BIG-2 [17]. In particular, it has been shown [13] that it may be possible to carry out an experiment at the upgraded SIS18 facility to study the problem of hydrogen metallization.

GSI is also planning to construct a new synchrotron ring SIS100, which will deliver a heavy ion beam with a much higher intensity as compared to the upgraded SIS18 facility. The availability of this beam will make many interesting experiments in the field of equation-of-state (EOS) studies possible [18].

Numerical simulations are an essential tool to design a future experiment efficiently and economically. On the other hand, after the experiments are performed, numerical simulation codes are needed to interpret the vast amount of experimental data. However, sophisticated simulation models are complicated and one needs to use analytic models to understand the large amount of numerical data generated by simulations. In addition to that, a good analytic model is always very helpful to optimize simulations as the model can qualitatively suggest the region of the parameter space in which one should start the simulations.

In order to supplement our numerical simulation capabilities, we have developed an analytic model to study the implosion of a multilayered cylindrical target that is driven by an intense heavy ion beam. In Sec. II we present the beam-target geometry and the necessary beam and target parameters, while the details of the model are given in Sec. III. The results obtained from the model together with a comparison with the simulation results are discussed in Sec. IV, while the conclusions drawn from this work are noted in Sec. V.

II. BEAM-TARGET PARAMETERS

In this section, we present the beam-target geometry of an experiment that will be carried out at the future GSI accel-

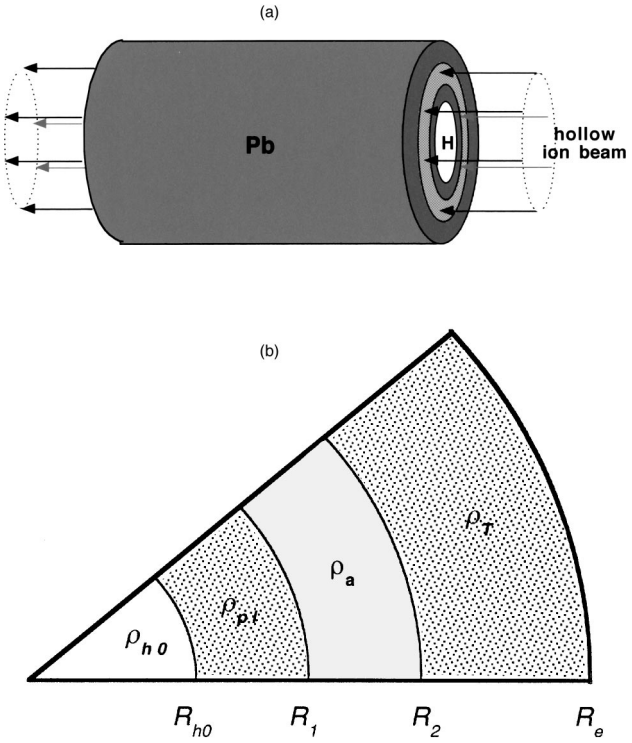

FIG. 1. (a) Beam-target geometry: a cylinder of solid hydrogen (H) enclosed in a shell of solid lead (Pb). (b) Sector of the layer-structured cylindrical target: ϱ_{h0} and R_{h0} are the density and radius of the solid hydrogen; $\varrho_{\rm pl}$ and R_1 are the density and the outer radius of the payload; ϱ_a and R_2 are the density and outer radius of the absorber and ϱ_T and R_e are the density and outer radius of the tamper, respectively.

erator facility. Figure 1(a) shows the proposed configuration and it is seen that the target is composed of a solid hydrogen cylinder with radius R_{h0} and density ϱ_{h0}, which is enclosed in a thick shell of solid lead. The right face of the target is irradiated with an ion beam that has an annular or a ring shaped focal spot. The inner radius of the focal ring, R_1, is assumed to be larger than R_{h0}, which avoids direct heating of the hydrogen. The outer radius of the focal spot ring, R_2, is considered to be much less than the outer radius of the lead shell, R_e. The region $R_2 \leqslant r \leqslant R_e$ acts as a tamper limiting the outward expansion of the absorption region. A cross sectional view of the target is shown in Fig. 1(b).

It is assumed that the length of the target is much less than the range of the projectile particles so that the energy deposition along the particle trajectory is fairly uniform. A shell of heated material with very high pressure is created in the absorber region lying between R_1 and R_2 with mass m_a and density ϱ_a, while the region lying between R_{h0} and R_1 forms a cold payload shell having mass $m_{\rm pl}$ and density $\varrho_{\rm pl}$. The hydrogen mass is denoted with m_h. In practice, one always has the condition $m_{\rm pl} \ll m_a$ fulfilled and in the cases of interest, one also has $m_h \ll m_{\rm pl}$.

The high pressure in the absorber generates a shock wave that travels through the payload and is then transmitted into the hydrogen. This shock travels along the radius of the hydrogen cylinder and is reflected at the axis. The reflected shock travels outward and is re-reflected by the payload. This process of multiple shock reflection goes on while the payload continues to move inwards, slowly compressing the hydrogen. This leads to a low entropy or ''cold compression'' of the hydrogen layer. Numerical simulations have shown [13,19] that using appropriate beam and target parameters, one can easily achieve the theoretically predicted physical conditions necessary for hydrogen metallization. These include a density of about 1 g/cm^3, a pressure of the order of 5 Mbars and a temperature of a few thousand Kelvin.

In this design, we consider the future SIS100 beam that will be composed of uranium ions. A wide range of particle energy, 400 MeV/*u* to 2.7 GeV/*u*, will be available and the pulse duration corresponding to the above energy range will be 90–20 ns. The maximum beam intensity is expected to be 2×10^{12} particles.

In these particular calculations we consider a particle energy of 2.7 GeV/*u* which has a range of about 6 cm in solid cold lead [20]. This allows us to take a very long target (2 cm) and still achieve a uniform deposition along the axial direction. If one chooses to use a lower energy, the target length should be decreased accordingly. The duration of the pulse in the present case is 20 ns.

Although the final maximum expected beam intensity is 2×10^{12}, the intensity will increase gradually over time. We therefore have used different cases with different beam intensities including 5×10^{10}, 10^{11}, 2×10^{11}, 4×10^{11}, 6×10^{11}, 8×10^{11}, and 10^{12} ions. These different beam intensities lead to very different values of specific energy deposition in lead that in turn leads to different implosion conditions in hydrogen. Therefore, use of different beam intensities would allow one to access a wide range of physical conditions of cold, compressed, high-pressure hydrogen and one may study the EOS properties of these exotic states of this most abundantly found element.

It is to be noted that we have used a hollow beam with an annular focal spot, and to generate such a beam is still a challenging problem. In the following, we discuss two possible methods that may be used to generate such a beam.

Generation of a hollow beam with an annular focal spot

It has been demonstrated that a beam geometry with an annular focal spot can be achieved in principle using a plasma lens [12]. However, producing a focal spot that provides a highly symmetrical intensity with the parameters used in these simulations requires a lot more research and developmental work.

Another proposal is to employ a high frequency wobbler that rotates the beam with a rotation frequency of the order of gigahertz, which would lead to an annular focus. In this case, it is very important to know the value of the rotation frequency that will be needed for an acceptable symmetry (of the order of a few percent) in the driving pressure, which is important for the target stability. A simple estimation of the required rotation frequency can be done as follows by considering a box pulse of power P and duration τ_p. In such a case, a region in the absorber with size of the order of the focal spot $r_{\rm fs}$ is heated by the rotating beam during a time of

the order of $t_c = r_{fs}/[\omega(R_1 + r_{fs})]$, where $\omega = 2\pi\nu$ is the angular velocity of rotation and ν is the frequency. During this time the pressure increases in such a region by $\Delta p \propto P t_c / r_{fs}^2$. On the other hand, the maximum pressure in the absorber is $p \propto P\tau_p/[(R_1+2r_{fs})^2 - R_1^2]$. Thus, the relative pressure asymmetry is $\Delta p/p \approx 4/(\omega\tau_p)$, independent of the target size. By requiring a pressure symmetry better than, for instance, 4% and taking $\tau_p \sim 30$ ns, it yields $\nu \geqslant 0.5$ GHz or a rotation period of less than 2 ns.

III. IMPLOSION MODEL

In this section we describe in detail the analytic model for the implosion of a multilayered cylindrical target driven by an intense ion beam. We assume that during the implosion the payload and absorber masses are not changed by thermal conduction. In fact, even for the largest specific internal energy of the absorber considered ($\sim$20 kJ/g), the thermal conductivity κ of the absorber remains very low ($\kappa \leqslant 5 \times 10^{-6}$ g/s cm) during the implosion time. Then, the thermal wave penetrates a very short distance l_c into the payload ($l_c \leqslant 10^{-7}$ cm) so that the heated payload mass that is incorporated to the absorber can be neglected.

On the other hand, we can also neglect the hydrogen and payload preheating produced by scattered absorber nuclei and by the secondary particles created when fast ions of the beam interact with the absorber material (electrons, photons, and nuclear fission fragments). By following the analysis of Ref. [21] we can see that for the beam deposition energies considered here, this preheating is small in comparison with the shock preheating.

A. Absorber expansion and shock transmission in the payload

When the absorber is heated by the ion beam, its pressure increases considerably and it pushes the payload inwards. For simplicity, we assume that the energy deposition in the radial direction is uniform. Since we are interested in the case in which the payload mass m_{pl} is much less than the absorber mass m_a ($m_{pl} \ll m_a$), the time taken by the rarefaction created at the payload surface to cross the absorber is longer compared to the implosion time. Thus, the payload implosion is driven by a simple rarefaction wave, as it happens in the classical Lagrange ballistic problem [22]. If the absorber is heated in a time much shorter than the characteristic hydrodynamic time required for its expansion, we can consider that the beam energy is deposited in the absorber instantaneously and thus one can assume that, at $t=0$, the absorber has a specific internal energy ϵ_0 which is equal to the total specific energy deposited by the ion beam. Therefore the instantaneous pressure $p_{pl}(t)$ on the payload surface can be calculated as [22]

$$p_{pl}(t) = p_0 \left(1 - \frac{\gamma_a - 1}{2} \frac{|\dot{R}|}{c_0} \right)^{2\gamma_a/(\gamma_a - 1)}, \tag{1}$$

$$p_0 = (\gamma_a - 1)\varrho_a \epsilon_0, \quad c_0 = \left(\frac{\gamma_a p_0}{\varrho_a} \right)^{1/2}, \tag{2}$$

where ϱ_a is the absorber density and we have assumed an ideal gas equation of state for the absorber with an enthalpy coefficient γ_a (which is equivalent to a Mie-Gruneisen EOS with a constant Gruneisen coefficient $\Gamma_a = \gamma_a - 1$). Besides, $\dot{R}$ is the instantaneous velocity of the interface payload absorber and c_0 is the speed of sound in the absorber.

The pressure p_{pl} drives a shock wave in the payload, which travels with velocity U_s:

$$U_s^2 \approx \frac{p_0}{2\varrho_{pl0}} \left[(\gamma_{pl} - 1)\frac{p_B}{p_0} + (\gamma_{pl} + 1) \right], \tag{3}$$

where γ_{pl0} is the enthalpy coefficient of the payload, ϱ_{pl0} is initial payload density, $p_B = B_{pl}/\gamma_{pl}$ (B_{pl} is the adiabatic bulk modulus of the payload) and we have taken $p_{pl} \approx p_0$ because during this stage the outer face of the payload moves relatively slowly. This shock arrives at the inner face of the payload at $t = t_0$ and enters into the hydrogen. At this time, the pressure within the payload is $p_{pl}(t_0) \approx p_0$ and the density is $\varrho_{pl}(t_0)$ given by

$$\varrho_{pl}(t_0) \approx \frac{(\gamma_{pl} - 1)\frac{p_B}{p_0} + (\gamma_{pl} + 1)}{(\gamma_{pl} + 1)\frac{p_B}{p_0} + (\gamma_{pl} - 1)} \varrho_{pl0}. \tag{4}$$

The entropy created by the shock places the payload on the isentrope S_0 given by

$$S_0 \approx \frac{p_0}{[\varrho_{pl}(t_0)]^{\gamma_{pl}}} = \frac{p_{pl}(t)}{[\varrho_{pl}(t)]^{\gamma_{pl}}}, \tag{5}$$

where p_{pl} is the mean value of the instantaneous pressure on the payload surface and we have assumed that the entropy created by this shock is conserved up to the stagnation phase.

On the other hand, at $t = t_0$ the fluid velocity U_{pl} behind the shock is given by

$$U_{pl}^2 \approx \frac{p_0}{\varrho_{pl}(t_0)} \frac{2\left(1 - \frac{p_B}{p_0}\right)^2}{(\gamma_{pl} - 1)\frac{p_B}{p_0} + (\gamma_{pl} + 1)}. \tag{6}$$

Since the payload entropy is assumed to be conserved for times $t_0 \leqslant t \leqslant t_2$, its internal energy E_{pl} evolves isentropically up to the time $t = t_2$, and it can be written as

$$E_{pl}(t) = \frac{m_{pl}}{(\gamma_{pl} - 1)} \frac{p_{pl}(t)}{\varrho_{pl}(t)}, \quad t_0 \leqslant t \leqslant t_2. \tag{7}$$

At $t = t_0$ a strong shock is launched into hydrogen, which arrives at the axis at $t = t_1$. It is then reflected, thereby compressing the hydrogen strongly. The reflected shock encounters the imploding inner face of the payload at $t = t_2$ and the stagnation phase starts. For $t > t_2$, shocks progressively become weaker and they are reflected between the axis and the pusher, leading to a nearly isentropic compression of the hydrogen. This compression continues up to the instant $t = t_f$,

when total stagnation occurs and the payload kinetic energy is converted into internal energy of the payload and of the hydrogen.

B. Payload implosion

At $t=t_0$ the payload starts to move inwards. We are interested in using a relatively thick pusher, therefore, the inner and the outer pusher radii move with different velocities. We then consider the implosion of a finite thickness shell, which is assumed to be incompressible. In principle, this assumption may appear to be inconsistent with the previous one regarding the isentropic evolution of the payload after $t=t_0$. However, for thick and heavy pushers, the motion is so slow that the pressure on the interface absorber-pusher changes very little and both assumptions are practically equivalent. For the opposite case of thin pushers, they move with a practically uniform velocity and the incompressibility assumption becomes irrelevant. Thus the payload implosion can be treated as incompressible without introducing significant errors. In such a case the continuity and momentum conservation equations read as

$$\frac{1}{r}\frac{\partial(vr)}{\partial r}=0, \tag{8}$$

$$\frac{\partial v}{\partial t}+v\frac{\partial v}{\partial r}=-\frac{1}{\varrho_{\rm pl}(t_0)}\frac{\partial p}{\partial r}. \tag{9}$$

These equations are easily integrated and yield

$$\dot{R}_h=\frac{R\dot{R}}{R_h}, \tag{10}$$

$$\frac{p_{\rm pl}(t)-p_h(t)}{\varrho_{\rm pl}(t_0)}=-(\ddot{R}R+\dot{R}^2)\ln\left(\frac{R}{R_h}\right)+\frac{\dot{R}^2}{2}\left(\frac{R^2}{R_2^2}-1\right), \tag{11}$$

where R_h and $\dot{R}_h$ are the instantaneous position and velocity of the inner radius of the payload, respectively. R, $\dot{R}$, and $\ddot{R}$ are the respective instantaneous position, velocity, and acceleration of the payload outer face. Also $p_h(t)$ is the counterpressure on the inner face produced by the material behind the shock that was launched into the hydrogen at $t=t_0$. Since the hydrogen density ϱ_{h0} is much less than the pusher density $[\varrho_{h0}\ll\varrho_{\rm pl}(t_0)]$, a strong shock propagates into the hydrogen and the averaged value of the counterpressure in the shocked region can be approximately calculated as

$$p_h(t)\approx\frac{2}{\gamma_{h1}+1}\varrho_{h0}\dot{R}_s^2, \quad t_0\leqslant t\leqslant t_1, \tag{12}$$

where γ_{h1} is the enthalpy coefficient of the shocked material and $\dot{R}_s$ is the instantaneous velocity of the shock launched into the hydrogen. For simplicity, we take constant values for the enthalpy coefficient of the hydrogen in the different phases of compression. Thus γ_{h1} is the effective value for the phase in which hydrogen is compressed by the incident shock ($t_0\leqslant t\leqslant t_1$). During this stage, the payload motion is described by Eqs. (10) and (11) with $p_{\rm pl}(t)$ and $p_h(t)$ given by Eqs. (1) and (12), respectively. Therefore, in order to find the payload trajectory and calculate the compression produced by the incident shock, we need to describe the shock motion in hydrogen.

C. Incident shock ($t_0\leqslant t\leqslant t_1$)

For the description of the incident shock we use a simple model which considers that a fixed mass of shocked material is compressed adiabatically by the motion of the piston (the inner face of the payload) [23,24]. Such an assumption implies that any change in the piston motion is immediately transmitted to the shock front and, therefore, their dynamics are always coupled. This leads to

$$p_hV_{h1}^{\gamma_{h1}}=\text{const}, \quad V_{h1}=\pi(R_h^2-R_s^2). \tag{13}$$

When the strong shock moves through a small distance dR_s, the fluid is compressed by a factor $(\gamma_{h1}+1)/(\gamma_{h1}-1)$. The new material incorporated behind the front occupies only a fraction $(\gamma_{h1}-1)/(\gamma_{h1}+1)$ of the increment of the volume $2\pi R_s dR_s$. Therefore, an extra volume that is a factor $2/(\gamma_{h1}+1)$ of such increment is available to the ''old'' mass between the shock and the piston. Consequently, the increment of volume dV_{h1} of the ''old'' material turns out to be

$$dV_{h1}=2\pi\left(R_h dR_h-\frac{2}{\gamma_{h1}+1}R_s dR_s\right). \tag{14}$$

Differentiating the first of Eqs. (13), we get

$$\frac{dp_h}{p_h}+\gamma_{h1}\frac{dV_{h1}}{V_{h1}}=0. \tag{15}$$

Using Eqs. (12) and (14) we obtain the equation of motion of the incident shock as

$$\ddot{R}_s=-\frac{\gamma_{h1}\dot{R}_s}{R_h^2-R_s^2}\left(R_h\dot{R}_h-\frac{2}{\gamma_{h1}+1}R_s\dot{R}_s\right). \tag{16}$$

Equations (10) and (11) [with Eq. (12)], and Eq. (16) represent a complete set of differential equations for the description of the payload and shock motion during the interval $t_0\leqslant t\leqslant t_1$, which must be solved with the following initial conditions at $t=t_0$:

$$R(t_0)=\left[\frac{m_{\rm pl}}{\pi\varrho_{\rm pl}(t_0)}+R_{h0}^2\right]^{1/2}, \quad \dot{R}(t_0)=\frac{R_{h0}U_{\rm pl}}{R(t_0)}, \tag{17}$$

$$R_h(t_0)=R_{h0}, \quad \dot{R}_h(t_0)\approx 2U_{\rm pl}, \tag{18}$$

$$R_s(t_0)=R_{h0}, \quad \dot{R}_s(t_0)=\frac{\gamma_{h1}+1}{2}\dot{R}_h(t_0), \tag{19}$$

where $\varrho_{\rm pl}(t_0)$ is given by Eq. (4) and $U_{\rm pl}$ is given by Eq. (6). Besides this, in the first of Eqs. (17) we have taken into account the shock compression in the payload, and in the

second of Eqs. (18) we have used the doubling rule for the velocity of a solid-vacuum interface when a shock emerges from the solid [25].

D. Reflected shock ($t_1 \leqslant t \leqslant t_2$)

At $t=t_1$, the incident shock is reflected at the axis and it propagates outwards with an instantaneous velocity $\dot{R}_{\rm sr}$ until $t=t_2$, when the shock hits the imploding piston. As a simple approximation, we adopt the expression corresponding to a planar shock for the mean value of the counterpressure p_h produced by the sample material ahead of the reflected shock. Then, the pressure of the fluid between the shock and the piston is written as [26]

$$p_h(t) \approx \frac{\gamma_{h1}+1}{2(\gamma_{h1}-1)(\gamma_{h2}-1)}\varrho_{h0}\dot{R}_{\rm sr}^2, \quad t_1 \leqslant t \leqslant t_2, \quad (20)$$

where γ_{h2} is the enthalpy coefficient of the hydrogen behind the reflected shock. At $t=t_2$, the mean pressure behind the shock can be expressed as

$$p_2 = \frac{3\gamma_{h2}-1}{\gamma_{h2}-1}p_h(t_2). \quad (21)$$

Following the same arguments as for the incident shock, we consider that a fixed mass of material behind the shock is adiabatically compressed but, now, we must take into account the fact that also the material ahead of the shock front is isentropically compressed as the payload implodes. One therefore writes

$$p_h V_{h2}^{\gamma_{h2}} = \text{const}, \quad V_{h2} = \pi R_h^2, \quad (22)$$

and the rate of change of volume for a fixed mass turns out to be

$$\frac{dV_{h2}}{dt} = 2\pi R_{\rm sr}\frac{\dot{R}_{\rm sr}-\dot{R}_h^0}{\gamma_{h2}} + 2\pi R_h\dot{R}_h, \quad \dot{R}_h^0 = \dot{R}_h\frac{R_h}{R_{\rm sr}}, \quad (23)$$

where $R_{\rm sr}$ is the instantaneous position of the reflected shock, and in writing the second of Eqs. (23) we have considered the conservation of the mass flux in the annular region between the shock and the piston. The effects of the geometry are also taken into account through Eqs. (22). Proceeding in a similar manner as for the incident shock, we get the following equation of motion for the reflected shock:

$$\ddot{R}_{\rm sr} = -\frac{\dot{R}_{\rm sr}}{R_h^2}[(\gamma_{h2}-1)R_h\dot{R}_h + R_{\rm sr}\dot{R}_{\rm sr}]. \quad (24)$$

This equation must be solved together with Eq. (11) for the motion of the piston with the counterpressure $p_h(t)$ given by Eq. (20) using the following initial conditions at $t=t_1$:

$$R_{\rm sr}(t_{1+}) = 0, \quad \dot{R}_{\rm sr}(t_{1+}) = \frac{2(\gamma_{h2}-1)}{\gamma_{h2}+1}\dot{R}_s(t_{1-}), \quad (25)$$

where $\dot{R}_s(t_{1-})$ is the velocity of the incident shock at $t=t_1$. The last equation is applied in order to ensure the continuity of the fluid velocity and pressure in the region between the shock and the piston at the instant of reflection at the axis. Besides this, the initial conditions for the piston at $t=t_1$ are obtained from the final conditions of the previous phase of incident shock (Sec. III C).

Equations (10) and (11) [now with Eq. (20)], and Eq. (24) provide the trajectory of the reflected shock. The calculation is stopped at $t=t_2$ when the shock hits the imploding piston. In this way, we can determine the pressure and the density of the sample $p_{h2}=p_h(t_2)$ and $\varrho_{h2}=\varrho_h(t_2)$, respectively. The pressure within the payload at this instant can be taken to be uniform and is equal to $p_{\rm pl2}=p_{\rm pl}(t_2)$. On the other hand, we obtain the payload kinetic energy E_{k2} and its internal energy $E_{\rm pl2}$ as well as the internal energy of the sample E_{h2}, which are given by the following expressions:

$$E_{k2} = \pi\varrho_{\rm pl}(t_0)R_2^2\dot{R}_2^2\ln\left(\frac{R_2}{R_{h2}}\right), \quad (26)$$

$$E_{\rm pl2} = \frac{m_{\rm pl}}{\gamma_{\rm pl}-1}\frac{p_{\rm pl2}}{\varrho_{\rm pl2}} \approx \frac{m_{\rm pl}}{\gamma_{\rm pl}-1}p_0^{(\gamma_{\rm pl}-1)/\gamma_{\rm pl}}S_0^{1/\gamma_{\rm pl}} \times\left(1-\frac{\gamma_a-1}{2}\frac{|\dot{R}|}{c_0}\right)^{[2\gamma_\alpha(\gamma_{\rm pl}-1)/\gamma_{\rm pl}]/[\gamma_{\rm pl}(\gamma_a-1)]}, \quad (27)$$

$$E_{h2} = -\frac{m_h}{\gamma_{h2}-1}\frac{p_{h2}}{\varrho_{h2}}, \quad (28)$$

where the subscript "2" denotes the values of the magnitudes at $t=t_2$ and $\varrho_{\rm pl2}$ is obtained from Eq. (5).

For $t \geqslant t_2$ the stagnation of the implosion takes place and the kinetic energy is converted into internal energy of the payload and of the sample. This phase is assumed to be practically isentropic.

E. Isentropic stagnation phase ($t_2 \leqslant t \leqslant t_f$)

Since the implosion stagnation is assumed to be isentropic, the following relationship exists between the pressure and the density of the sample for $t_2 \leqslant t \leqslant t_f$:

$$p_h = p_{h2}\left(\frac{\varrho_h}{\varrho_{h2}}\right)^{\gamma_{h3}}, \quad (29)$$

where γ_{h3} is the corresponding enthalpy coefficient of the sample in this phase.

In order to obtain the values $p_{hf}=p_h(t_f)$ and $\varrho_{hf}=\varrho_h(t_f)$ for the hydrogen pressure and density at maximum compression, we consider that the kinetic energy E_{k2} of the payload is completely converted into internal energy of the sample and of the payload:

$$E_{k2} = \Delta E_{\rm pl} + \Delta E_h, \quad (30)$$

where $\Delta E_{\rm pl}=E_{{\rm pl}f}-E_{\rm pl2}$ and $\Delta E_h=E_{hf}-E_{h2}$ (the subscript "f" denotes values at $t=t_f$).

For the calculation of the internal energy $E_{{\rm pl}f}$, we need to find the pressure and density profiles within the payload [27]. For this purpose, we use the well known self-similar solution

for the homogeneous isentropic compression of a cylindrical shell [28]. In such a model the momentum and mass conservation equations are solved together with Eq. (5),

$$\frac{d\varrho_{\rm pl}}{dt}+\frac{\varrho_{\rm pl}}{r'}\frac{\partial(vr')}{\partial r'}=0, \tag{31}$$

$$\varrho_{\rm pl}\frac{dv}{dt}=-\frac{\partial p_{\rm pl}}{\partial r'}, \tag{32}$$

and the following ansatz are proposed:

$$r'=rf(t), \quad v=r\dot{f}(t). \tag{33}$$

The previous equations lead to the following ordinary differential equations:

$$\ddot{f}f^{2\gamma_{\rm pl}-1}=\frac{1}{\tau^2}, \tag{34}$$

$$\frac{dp_{\rm pl}}{dr}=-\frac{\varrho_{\rm pl}r}{\tau^2}, \tag{35}$$

where τ is a characteristic time for the stagnation phase. Introducing Eq. (5) into Eq. (32) and using the following boundary conditions at $t=t_f$:

$$p_{{\rm pl}f}(R_{{\rm pl}f})\approx 0, \quad p_{{\rm pl}f}(R_{hf})=p_{hf}, \tag{36}$$

($R_{{\rm pl}f}$ is the outer radius of the payload at total stagnation) we can integrate Eq. (35) for obtaining the pressure and density profiles at $t=t_f$ which leads to

$$p_{{\rm pl}f}(r)\approx p_{hf}\left(\frac{R_{{\rm pl}f}^2-r^2}{R_{{\rm pl}f}^2-R_{hf}^2}\right)^{\gamma_{\rm pl}/(\gamma_{\rm pl}-1)}, \tag{37}$$

$$\varrho_{{\rm pl}f}(r)\approx\left(\frac{p_{hf}}{S_0}\right)^{1/\gamma_{\rm pl}}\left(\frac{R_{{\rm pl}f}^2-r^2}{R_{{\rm pl}f}^2-R_{hf}^2}\right)^{1/(\gamma_{\rm pl}-1)}. \tag{38}$$

From the previous equations we can obtain the internal energy of the payload by performing the corresponding mass and energy integrals for obtaining [27]

$$E_{{\rm pl}f}=\frac{m_{\rm pl}\gamma_{\rm pl}}{(\gamma_{\rm pl}-1)(2\gamma_{\rm pl}-1)}p_{hf}^{(\gamma_{\rm pl}-1)/\gamma_{\rm pl}}S_0^{1/\gamma_{\rm pl}}. \tag{39}$$

On the other hand, the internal energy of the sample at $t=t_f$ turns out to be

$$E_{hf}=\frac{m_h}{\gamma_{h3}-1}\frac{p_{hf}}{\rho_{hf}}. \tag{40}$$

Substituting Eqs. (26)–(28) and Eqs. (39) and (40) into Eq. (30) for the energy balance, and taking into account that the compression evolves isentropically [Eq. (29)], we can calculate the final pressure p_{hf} and density ϱ_{hf} of the sample.

TABLE I. Relevant target and beam parameters used in the model.

Specific energy deposition	ϵ_0 (kJ/g)	5
Sample density (hydrogen)	ϱ_{h0} (g/cm^3)	0.0886
Payload density (lead)	ϱ_{pl0} (g/cm^3)	11.30
Absorber density (lead)	ϱ_a (g/cm^3)	11.30
Hydrogen radius	R_{h0} (cm)	0.04
Inner radius of the focal spot	R_1 (cm)	0.06
Outer radius of the focal spot	R_2 (cm)	0.16
Absorber enthalpy coefficient	γ_a	1.72
Payload bulk modulus	$B_{\rm pb}$ (Mbar)	0.45
Payload enthalpy coefficient	$\gamma_{\rm pl}$	3.77
Hydrogen enthalpy coefficient (phase 1)	γ_{h1}	3.60
Hydrogen enthalpy coefficient (phase 2)	γ_{h2}	3.30
Hydrogen enthalpy coefficient (phase 3)	γ_{h3}	3.00

IV. RESULTS OF THE MODEL AND DISCUSSION

In order to apply the model to a particular case, we have considered as a first step the target and beam parameters shown in Table I. The target consists of a thick cylindrical shell of lead which is surrounding a sample of frozen hydrogen (Fig. 1).

The absorber enthalpy coefficient γ_a is determined from the simulations by looking at the value of the pressure just at the end of the pulse (pulse duration $\tau_p=20$ ns), when the absorber remains still at rest and has an initial density ϱ_a. The payload enthalpy coefficient $\gamma_{\rm pl}$ and the adiabatic bulk modulus $B_{\rm pl}$ are taken from Ref. [29]. Since the enthalpy coefficient of hydrogen depends on the compression factor, we have taken an effective constant value for each stage which is fitted from the realistic equation of state. For the largest compression factors ($4<\varrho/\varrho_{h0}<10$), the value is equal to that used by other authors ($\gamma_{h3}\approx 3$) [30], but it becomes somewhat larger for smaller compression, as seen by following an isentrope in the simulations.

The results of the model have been compared with one-dimensional simulations performed by using a one-dimensional mode of the two-dimensional hydrodynamic code BIG-2 [19]. In Fig. 2 we present the trajectories of the piston and of the incident and reflected shocks as given by the model (lines) and by the simulations (dots). It is seen that the model reproduces the simulation results very well.

Considering the target and beam parameters shown in Table I, we have performed a parametric analysis by changing the payload mass, the hydrogen mass, and the specific energy deposited by the beam.

In Fig. 3 we plot the final hydrogen pressure p_{hf} vs the payload mass for two different values of the specific energy, ϵ_0, namely, 5 and 10 kJ/g, respectively. It is seen that the higher value of ϵ_0 leads to higher values of pressure, which is an expected result. It is also seen that for the values of $m_{\rm pl}$ between 30 and 200 mg/cm, p_{hf} changes only slightly. We can calculate the final pressure of the hydrogen at the limit of very large payload mass, even if the model becomes invalid at the limit $m_{\rm pl}\sim m_a$:

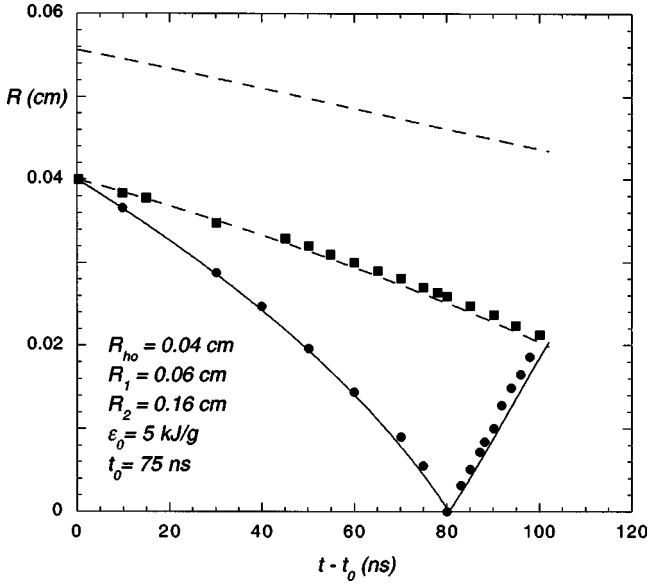

FIG. 2. Trajectories of the incident and first reflected shocks and of the inner and outer faces of the payload. Lines represent the results of the model and dots are obtained from 1D simulations.

$$p_{hf} \approx \left(\frac{2\gamma_{\rm pl} - 1}{\gamma_{\rm pl}} \right)^{(\gamma_{\rm pl}-1)/\gamma_{\rm pl}} p_0 . \tag{41}$$

For the case we are considering, it yields a minimum value of $p_{hf} \approx 0.6$ Mbars. The same behavior is also observed in simulations (dots) but for values of the pressures and densities somewhat different.

In the opposite case of very small masses of the payload, the final pressure decreases more abruptly. This is because the maximum velocity of the piston is limited to the value $2c_0/(\gamma_a - 1)$, determined by the absorber rarefaction and

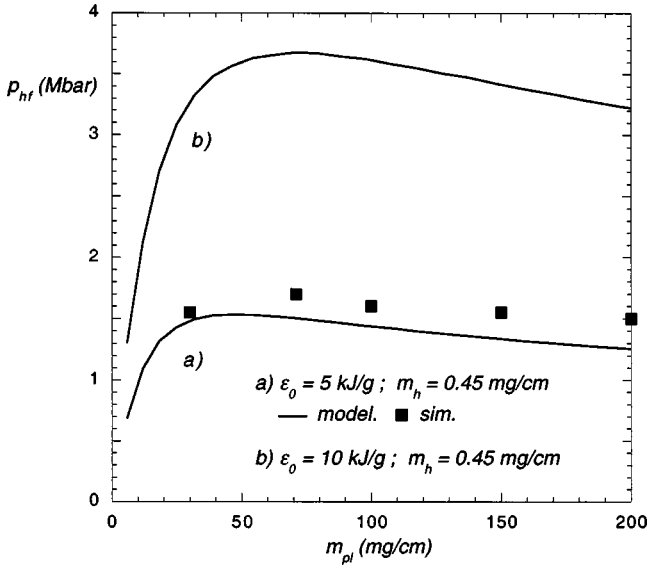

FIG. 3. Hydrogen pressure p_{hf} at stagnation as a function of the payload mass. (a) Beam deposition energy $\epsilon_0 = 5$ kJ/g; the line represents the model results and dots are obtained by 1D simulations. (b) Beam deposition energy $\epsilon_0 = 10$ kJ/g.

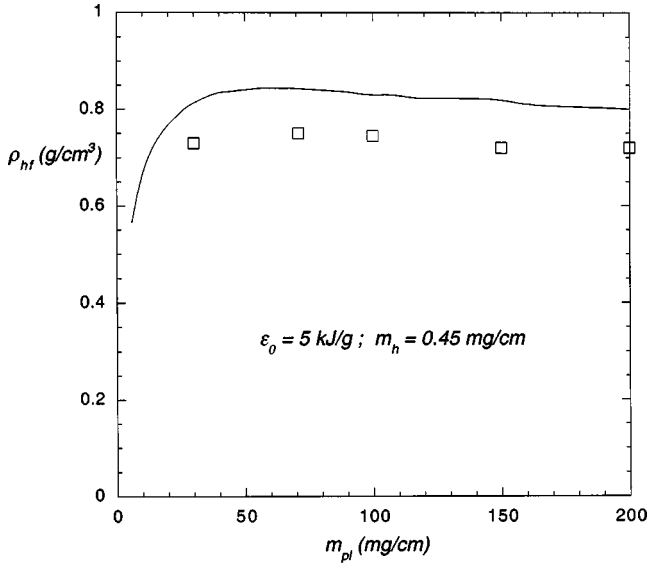

FIG. 4. Hydrogen density ϱ_{hf} at stagnation as a function of the payload mass for a beam deposition energy of $\epsilon_0 = 5$ kJ/g; the line represents the model results and dots are obtained by 1D simulations.

then the maximum kinetic energy decreases with the mass. At the limit, the final isentropic phase practically does not exist and the maximum compression is reached close to the time $t = t_2$, when the reflected shock encounters the imploding piston. Therefore $p_{hf} \approx p_{h2}$ and for the case under consideration we have $p_{hf} \approx 0.1$ Mbars. Nevertheless, it is worth noting that in practice the situation of zero payload mass will never occur. In fact, in the case where initially the payload would be very small, the fast expansion of the absorber would create a region not directly heated by the beam that would act as an effective payload. Such a situation cannot happen in our model because of the assumption of instantaneous heating.

Figure 4 shows the corresponding final hydrogen density values. It is seen that the density also shows an insensitivity to changes in $m_{\rm pl}$ in a similar manner as the pressure. This is a very important result as such an insensitivity would allow one to use a practically arbitrary radial profile for the beam energy deposition. This profile will determine the effective payload mass without affecting the implosion dynamics. However a suitable deposition profile can create a smooth density profile between the payload and the absorber with a characteristic scale length of the order of the absorber thickness, which is certainly of great importance for reducing the instability growth rate during the implosion.

In Fig. 5 we plot the final hydrogen pressure and density vs ϵ_0; solid line represents the model predictions while the squares are the simulation results. These results show that the model predicts a variation in p_{hf} according to the scaling law given below

$$p_{hf}\ ({\rm Mbar}) \approx 0.24[\,\epsilon_0\ ({\rm kJ/q})\,]^{1.176}. \tag{42}$$

In this case the simulation results and the model predictions are in good agreement.

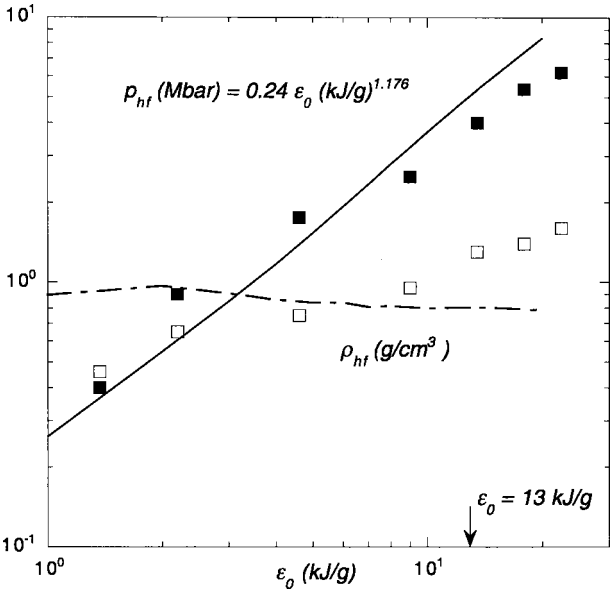

FIG. 5. Hydrogen pressure p_{hf} and density ϱ_{hf} at stagnation as functions of the specific energy ϵ_0 deposited by the beam. Lines are given by the model. Filled squares represent the pressure and hollow squares represent the density given by simulations.

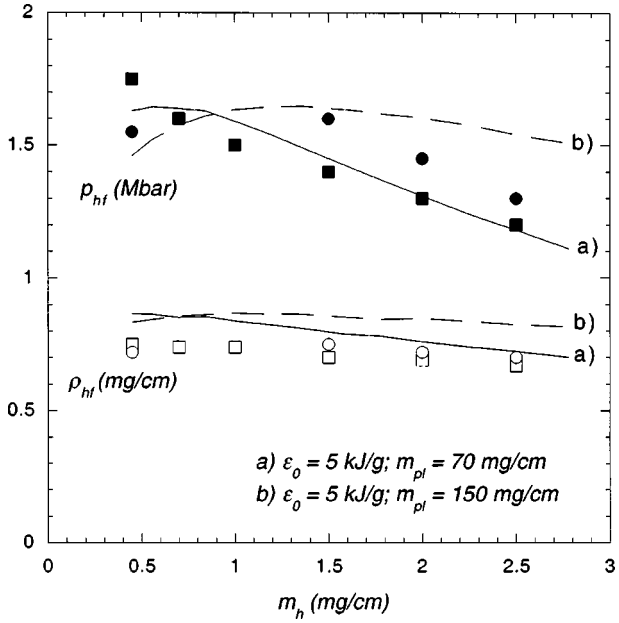

FIG. 6. Hydrogen pressure p_{hf} and density ϱ_{hf} at stagnation as functions of the hydrogen mass m_h for a beam deposition energy of $\epsilon_0 = 5$ kJ/g. (a) Payload mass $m_{\mathrm{pl}} = 70$ mg/cm, lines are calculated with the model and square dots are given by simulations. (b) Payload mass $m_{\mathrm{pl}} = 150$ mg/cm, lines are calculated with the model and circle dots are given by simulations.

However, according to the model, the density is practically independent of the beam specific energy deposition while the simulations show that it increases with energy as $\varrho_{hf} \propto \epsilon_0^{0.4}$. Such a difference may be a consequence of the simple hydrogen equation of state used in the model but is of minor relevance for the application of the model in optimizing the simulations. In Fig. 5 we have also indicated the minimum value of the specific energy deposition $\epsilon_0 \approx 13$ kJ/g required to achieve the theoretically predicted conditions necessary for hydrogen metallization ($p_{h0} \geqslant 5$ Mbar and $\varrho \geqslant 1$ g/cm^2).

Another interesting result is shown in Fig. 6 where we have presented the final pressure and density that is reached in the hydrogen as a function of the hydrogen mass for two different payload masses (keeping constant the specific energy $\epsilon_0 = 5$ kJ/g). Model and simulations show no changes in the final density and a slight reduction (around 20%) in the final pressure when the hydrogen mass is increased from 0.5 to 2 mg/cm. This result allows for the design of relatively large size targets ($R_h \sim 1$ mm), using a given specific energy deposition that may represent an advantage for the experimental diagnostics, because of the large dimensions of the compressed sample.

In summary this design can tolerate substantial variations in the beam and target parameters, without any significant changes in the final conditions of the hydrogen sample.

V. CONCLUDING REMARKS

We have used the analytical model presented in this paper to study a heavy ion driven implosion of a multilayered target made up of a solid hydrogen cylinder enclosed in a solid lead shell. This type of experiment will be carried out at the GSI accelerator facility in the future. Our model successfully describes the trajectories of the payload and of the incident and reflected shocks, which determine the initial conditions for the stagnation phase. The final stagnation is treated as an isentropic compression.

We have carried out analysis using a wide range of target and beam parameters. The target parameters including the hydrogen mass and the payload mass are varied parametrically while keeping the specific energy deposition constant. In other cases we varied the specific energy deposition, keeping the target parameters fixed. This parameter study has shown that the final physical conditions that can be achieved in hydrogen are fairly insensitive to substantial variations in the target and beam parameters, which means a very robust target design.

Moreover, this allows one to use a larger hydrogen mass for the same driving energy. This will lead to the creation of a larger sample of compressed hydrogen at the end of the implosion, which is good for diagnostics purposes.

The model results have been compared with numerical simulations using a one-dimensional mode of the sophisticated two-dimensional code BIG-2. The model predictions show reasonably good agreement with the simulation results.

ACKNOWLEDGMENTS

The authors wish to thank M. Temporal and G. Wouchuk for very helpful discussions. One of us (A.R.P.) would like to thank the staff of the Heavy Ion Plasma Physics Group at the GSI Darmstadt for their hospitality during his one month stay at GSI. This work was financially supported by the BMBP (Germany) and the Consejería de Ciencia y Technología—JCCM-PAI-02-002 (Spain).

[1] E. Wigner and H. B. Huntington, J. Chem. Phys. **3**, 764 (1935).
[2] H. K. Mao and R. J. Hemley, Rev. Mod. Phys. **66**, 671 (1994).
[3] S. T. Weir, A. C. Mitchell, and W. J. Nellis, Phys. Rev. Lett. **76**, 1860 (1996).
[4] W. J. Nellis, A. C. Mitchell, P. C. McCandles, D. J. Erskine, and S. T. Weier, Phys. Rev. Lett. **68**, 2937 (1992).
[5] V. E. Fortov, V. Ya. Ternovoi, S. V. Kvitov, V. B. Mintsev, D. N. Nicolaev, A. A. Pyalling, and A. S. Filiminov, JETP Lett. **69**, 926 (1999).
[6] C. Narayan, H. Luo, J. Orlof, and A. L. Ruoff, Nature (London) **393**, 46 (1998).
[7] N. W. Ashcraft, Phys. Rev. Lett. **21**, 1784 (1968).
[8] A. Ng and A. R. Piriz, Phys. Rev. A **40**, 1993 (1988).
[9] D. H. H. Hoffmann *et al.*, Phys. Rev. A **42**, 2313 (1990).
[10] S. Stöwe *et al.*, Nucl. Instrum. Methods Phys. Res. A **415**, 384 (1998).
[11] U. Funk *et al.*, Nucl. Instrum. Methods Phys. Res. A **415**, 68 (1998).
[12] U. Neuner *et al.*, Phys. Rev. Lett. **85**, 4518 (2000).
[13] D. Varentsov *et al.*, Nucl. Instrum. Methods Phys. Res. B **174**, 215 (2001).
[14] N. A. Tahir *et al.*, Phys. Rev. E **61**, 1975 (2000).
[15] N. A. Tahir *et al.*, Phys. Rev. E **62**, 1224 (2000).
[16] N. A. Tahir *et al.*, Phys. Rev. E **63**, 016402 (2001).
[17] V. E. Fortov *et al.*, Nucl. Sci. Eng. **123**, 169 (1996).
[18] D. H. H. Hoffmann *et al.*, Phys. Plasmas (to be published).
[19] N. A. Tahir *et al.*, Contrib. Plasma Phys. **41**, 287 (2001).
[20] J. F. Ziegler *et al.*, *The Stopping and Ranges of Ions in Solids* (Pergamon, New York, 1996).
[21] M. M. Basko, Laser Part. Beams **10**, 189 (1995).
[22] K. P. Stanyukovich, *Unsteady Motion of Continuous Media* (Pergamon, London, 1960).
[23] D. Potter, Nucl. Fusion **18**, 813 (1978).
[24] A. R. Piriz, G. E. Giudice, and F. G. Tomasel, Phys. Fluids B **4**, 693 (1992).
[25] Ya. B. Zeldovich and Yu. P. Raizer, *Physics of Shock Waves and High-Temperature Hydrodynamic Phenomena* (Academic, London, 1967), Vol. II.
[26] L. D. Landau and E. M. Lifshits, *Fluid Mechanics*, 2nd ed. (Pergamon, Oxford, 1987).
[27] A. R. Piriz, Phys. Fluids **29**, 578 (1986).
[28] R. E. Kidder, Nucl. Fusion **16**, 3 (1976).
[29] J. F. Barnes, Phys. Rev. **153**, 269 (1967).
[30] S. I. Anisimov, JETP Lett. **16**, 404 (1972).